



Detection of Potential Vernal Pools on the Canadian Shield (Ontario) Using Object-Based Image Analysis in Combination with Machine Learning

Nick Luymes & Patricia Chow-Fraser

To cite this article: Nick Luymes & Patricia Chow-Fraser (2021) Detection of Potential Vernal Pools on the Canadian Shield (Ontario) Using Object-Based Image Analysis in Combination with Machine Learning, Canadian Journal of Remote Sensing, 47:4, 519-534, DOI: [10.1080/07038992.2021.1900717](https://doi.org/10.1080/07038992.2021.1900717)

To link to this article: <https://doi.org/10.1080/07038992.2021.1900717>



Published online: 06 May 2021.



Submit your article to this journal [↗](#)



Article views: 112



View related articles [↗](#)



View Crossmark data [↗](#)



Detection of Potential Vernal Pools on the Canadian Shield (Ontario) Using Object-Based Image Analysis in Combination with Machine Learning

Détection des étangs vernaux potentiels sur le Bouclier canadien (Ontario) à l'aide d'une analyse orientée objet en combinaison avec l'apprentissage automatique

Nick Luymes  and Patricia Chow-Fraser 

Department of Biology, McMaster University, Hamilton, ON L8S 4L8, Canada

ABSTRACT

Vernal pools are small, temporary, forested wetlands of ecological importance with a high sensitivity to changing climate and land-use patterns. These ecosystems are under considerable development pressure in southeastern Georgian Bay, where mapping techniques are required to inform wise land-use decisions. Our mapping approach combines common machine learning techniques [random forest, support vector machines (SVMs)] with object-based image analysis. Using multispectral image segmentation on high-resolution orthoimagery, we first created objects and assigned classes based on field collected data. We then supplied machine learning algorithms with data from freely available sources (Ontario orthoimagery and Sentinel 2) and tested accuracy on a reserved dataset. We achieved producer's accuracies of 85 and 79% and user's accuracies of 78 and 84% for random forest and SVMs models, respectively. Difficulty differentiating between small, dark shadows and small, obscured pools accounted for many of the omission and commission errors. Our automated approach of vernal pool classification provides a relatively accurate, consistent, and fast mapping strategy compared to manual photointerpretation. Our models can be applied on a regional basis to help verify the locations of pools in an area of Ontario that is in critical need of more detailed ecological information.

RÉSUMÉ

Les étangs vernaux sont de petites zones humides forestières temporaires d'importance écologique très sensibles aux changements climatiques et aux modes d'utilisation des terres. Ces écosystèmes sont soumis à une pression de développement considérable dans le sud-est de la Baie Georgienne, où des techniques de cartographie sont nécessaires pour éclairer les décisions en matière d'utilisation des terres. Notre approche de cartographie combine des techniques d'apprentissage automatique courantes (forêt aléatoire, machines à vecteurs de support) avec une méthode orientée-objet. En utilisant la segmentation multispectrale d'une image haute résolution ortho-rectifiée, nous avons créé des objets et attribué des classes en fonction des données collectées sur le terrain. Ensuite, nous avons fourni aux algorithmes d'apprentissage automatique des images disponibles gratuitement (Ontario orthoimagerie et Sentinel 2) et testé la précision sur un ensemble de données réservé. Nous avons obtenu des précisions de producteur de 85% et 79% et des précisions d'utilisateur de 78% et 84% pour les modèles de forêt aléatoire et machines à vecteurs de support, respectivement. La difficulté de distinguer les petites zones d'ombre des petits étangs obscurs est à l'origine de plusieurs des erreurs d'omission et de commission. Notre approche automatisée de classification des étangs vernaux fournit une stratégie de cartographie relativement précise, cohérente et rapide par rapport à la photo-interprétation manuelle. Nos modèles peuvent être appliqués sur une base régionale pour aider à vérifier l'emplacement des étangs dans une région de l'Ontario qui a un besoin critique d'informations écologiques détaillées.

ARTICLE HISTORY

Received 2 September 2020
Accepted 5 March 2021

Introduction

Temporary wetlands act as critical breeding habitats for amphibians across the globe and are increasingly being recognized for their disproportionate benefits to local biodiversity (Calhoun et al. 2017). In the Pleistocene glaciated part of northeastern North America, temporary wetlands commonly occur as small seasonally available, forested wetlands known as vernal pools. Vernal pools fill with water during the spring or fall and dry in the summer or in drought years. Their ephemeral nature precludes the establishment of permanent fish populations, allowing amphibian larvae and other aquatic species to avoid intense predation. Obligate vernal pool species, including Ambystomatid salamanders (*Ambystoma* sp.) and wood frogs (*Lithobates sylvaticus*), have optimal breeding success and recruitment in these fish-free habitats (Cormier et al. 2003; Semlitsch et al. 2015). These obligate amphibians, and the many facultatively breeding amphibians that frequent vernal pools, are of conservation interest due to their sensitivity to environmental stressors (Semlitsch and Brodie 1998), importance in forest energy and nutrient cycling (Leibowitz 2003), and the fact that some are considered species at risk.

Vernal pools are necessary for the maintenance of local amphibian populations (Leibowitz 2003), but their small size and ephemeral nature often means they are overlooked in wetland legislation (Evans et al. 2017). In Ontario, most vernal pools are ineligible for protection under the Ontario Wetland Evaluation System's current guidelines for provincially significant wetlands (Ontario Ministry of Natural Resources and Forestry 2014). Consequently, they are unlikely to factor into land-use decisions and can face habitat degradation and loss of landscape connectivity as a result (Calhoun et al. 2017). The anticipated effects of climate change, including shorter and less frequent hydroperiods (Brooks 2009), further highlight the need for improved management of vernal pools in the province.

Knowledge of the location and distribution of vernal pools is essential to their protection; however, the canopy-obstructed nature of these wetlands complicates mapping efforts. Techniques for large-scale wetland mapping, including the National Wetland Inventory (NWI), are often unfeasible for vernal pools because the pools are either too small to be reasonably detected or are obscured by overhead forest canopy cover (Baldwin and deMaynadier 2009). Several geopolitical entities within the northeastern United States have developed regulatory protections for vernal

pools, which has led to state-wide efforts to map and document vernal pools (e.g. Brooks et al. 1998; Faccio et al. 2013; Jansujwicz et al. 2013; Lathrop et al. 2005). The most common technique used to map vernal pools has been photointerpretation of high-resolution aerial imagery. While easy to implement, photointerpretation often results in highly variable accuracy and can be hindered by interpreter bias and skill (Carpenter et al. 2011).

Recent advances in remote-sensing technology and classification techniques have led to novel strategies for wetland mapping. Object-based image analysis (OBIA), in particular, has emerged in response to the increasing availability of high-resolution remote sensing data. OBIA involves grouping pixels together based on spectral similarities to form image objects, which can then be analyzed using spatial statistical models. While traditional pixel-based image analysis methods focus solely on the spectral characteristics of individual pixels, OBIA allows for the integration of object shape, texture, and neighborhood characteristics in addition to a greater range of spectral properties. OBIA has proven to be especially useful for the classification of high-resolution imagery, where features on the ground (e.g. wetlands, buildings, trees) tend to be represented better by image objects rather than individual pixels (Blaschke 2010). Wetland classification studies using OBIA have had success both with medium-resolution and high-resolution data (Amani et al. 2017; Dronova 2015; Grenier et al. 2008; Rampi et al. 2014; Tian et al. 2016), and comparisons with pixel-based approaches have shown that OBIA consistently produces more accurate results (Amani et al. 2017; Dronova 2015; Fu et al. 2017; Harken and Sugumaran 2005). Since the detection of small wetlands like vernal pools necessitates the use of high-resolution imagery, we consider OBIA a promising approach to vernal pool mapping.

For the information extracted from OBIA to be used for image classification, the data are often subjected to different machine learning classifiers, including k-nearest neighbor (KNN), classification and regression trees (CART), random forests (RF), support vector machines (SVM), and neural networks (NNs). These classifiers are able to handle many types of input data types without making assumptions on the data distributions, making them well suited for the diverse arrays of features extracted in OBIA. Machine learning classifiers have also been shown to consistently outperform conventional classifiers, such as maximum likelihood, and are becoming easier to implement as more image-processing programs

integrate machine learning algorithms into their software (Maxwell et al. 2018). Two of the most common machine learning algorithms used in remote sensing applications are RF and SVM. RF is an ensemble learning technique that uses a large number of decision trees to “vote” on class predictions. Each decision tree is constructed using a random subset of the data and predictor variables, resulting in a low correlation between the individual trees and reducing the chance of overfitting the data. SVM is a supervised machine learning classifier that uses multidimensional hyperplanes to maximize the width of decision margins between classes. It uses kernels to map features to higher dimensional space where linear separation is more effective. RF and SVM classifiers do not make formal distributional assumptions but require that the sampled data be representative. Since both classifiers are unable to extrapolate, they are limited in their predictive capabilities and have difficulty classifying data that are not averages of data encountered in model training. Machine learning classifiers can also be computationally intensive but advances in computing capabilities have made this less of an issue, resulting in more widespread use. Studies involving the classification of wetland landcover have had success with RF (Fu et al. 2017; Millard and Richardson 2013; Tian et al. 2016) and SVM classifiers (Amani et al. 2017; Chatziantoniou et al. 2017), and a study involving synthetic aperture radar data was able to map vernal pool locations using RF classifiers (Bourgeau-Chavez et al. 2016).

Many of the previously developed approaches to vernal pool mapping have involved the use of light detection and ranging data (LiDAR; Julian et al. 2009; Leonard et al. 2012; Riley et al. 2017; Wu et al. 2014). LiDAR systems allow the penetration of forest canopies and can be used to identify landscape depressions and the presence of water (Lang and McCarty 2009), both of which are crucial for vernal pool detection. Despite the clear benefits of LiDAR data to vernal pool mapping, many remote areas do not have access to the technology because of its high cost.

In this study, we are interested in mapping vernal-pool habitat in a remote area of south-central Ontario, where LiDAR data are not available, and where no large-scale vernal-pool mapping efforts have been attempted. Due to its pristine nature and proximity to Georgian Bay, this region is highly coveted by cottagers and, despite its mostly undisturbed state, is experiencing high development pressure. Therefore, there is an urgency in mapping critical habitat for amphibians and turtles, such as vernal pools, and

incorporating such information into official plans of the affected municipalities. Given these constraints, our goal was to develop an automated classification approach using freely available image products, and recent advances in image analysis technology. This is the first regional mapping effort of vernal-pool habitat in a mostly forested portion of Ontario, which is rapidly becoming altered by cottage and urban development. These maps will identify areas that should be targeted for intensive field surveys and ground truthing. Since similar remote sensing datasets are available for other unmapped regions of Ontario, we recommend using this approach to create a provincial database of potential vernal pools (PVPs) to guide effective land-use planning and wildlife conservation.

Methods

Field methods

Our region of interest for this study was the forested southeastern shore of Georgian Bay, Lake Huron, Ontario. This region is part of the Canadian Shield ecozone of Ontario and consists of a mixed coniferous-deciduous forest interwoven by numerous outcrops of exposed igneous bedrock (Crins et al. 2009). The climate is temperate and humid with an average annual precipitation of 950 mm and an average summer rainfall of 250 mm. The mosaic of exposed bedrock creates numerous depressions in the landscape for waterbodies to form, including lakes, thicket swamps, fens, ponds, and vernal pools. This region includes three vernal pool obligate amphibians (*Ambystoma laterale*, *A. maculatum*, *Lithobates sylvaticus*), as well as several species at risk that derive food, water, and shelter from vernal pools (e.g. *Clemmys guttata*, *Emydoidea blandingii*).

To collect our reference dataset of vernal pools, we selected six study sites (ranging in size from 25 to 175 ha; GB1, GB2, GB3, GB4, GB5, and GB6; Figure 1) located within 20 km of the shoreline of eastern Georgian Bay. These sites were selected based on three main criteria: (1) proximity to all-season roads for safe access by the survey team, (2) location on publicly accessible Crown Land, and (3) inclusion in the region of interest. Each study site was divided into one to seven 25-ha plots, depending on the overall site size. Based on available time and resources, we were able to conduct intensive field surveys in a total of 23 plots within the 6 study sites. All plots were surveyed during spring in 2016, 2018, or 2019.

In advance of the field sampling, we imported shapefiles of water bodies and wetlands prepared by

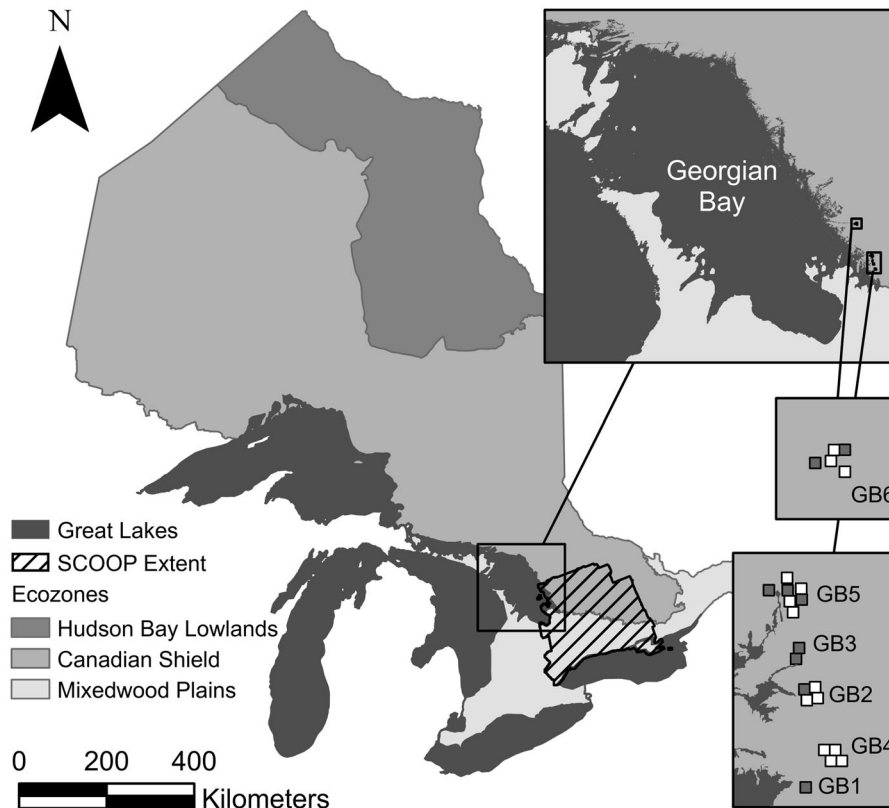


Figure 1. Location of the 23 sampling plots in the six sites (GB1, GB2, GB3, GB4, GB5, and GB6) in the Canadian Shield ecozone of Ontario, Canada. Plots used for model training are depicted as white squares, while plots used for validation are depicted as gray squares. The extent of the orthoimagery used in the study is shown with hatched markings. SCOOP: South Central Orthophotography Project.

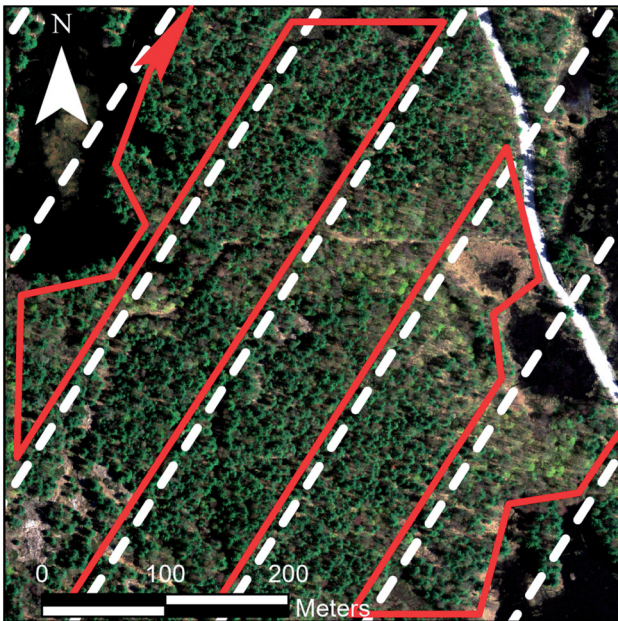


Figure 2. Example of a plot with transects (dashed lines) and the route taken by surveyors (solid line) to follow the transects while avoiding major barriers, such as roads and lakes. Basemap source: Ontario Ministry of Natural Resources and Forestry.

the Ontario Ministry of Natural Resources and Forestry (OMNRF) into ESRI Arc Collector application on an Apple™ iPad. We also imported the location of the 23 plots and created transects spaced at 100-m intervals in each plot (Figure 2). Transects in each plot were oriented to minimize encounters with barriers (e.g. large lakes, roads, ledges) and inter-transect spacing was determined based on estimated field of view during leaf-off conditions. We uploaded all transects to handheld GPS devices and walked at a moderate pace along the transects as shown in Figure 2. This allowed us to see all water bodies that were located on both sides of the transects. If the field of view was obstructed by hilly terrain, we walked up these inclines to ensure no wetlands were obscured. Whenever we encountered an undocumented wetland, we traced the outline of the wetland by foot and used Arc Collector application to record the information. Large wetlands and water bodies that had been documented by the Ontario Ministry of Natural Resources and Forestry (OMNRF) were not traced, but we noted any major areas that had been omitted. We continued in this way until the boundaries of all wetlands and

Table 1. Description of datasets and how they were used in this study.

Data set	Coverage	Resolution	Acquisition dates	Used to
Sentinel 2	Worldwide	10 m	April 27, 2016 May 7, 2018 May 5, 2019 NA	Screen areas of interest for classification; derive features for model development
Ontario Ministry of Natural Resources and Forestry (OMNRF) Wetlands/Waterbodies	Ontario-wide	NA	NA	Refine areas of interest for classification
South Central Ontario Orthophotography Project (SCOOP) true color/near-infrared imagery	~36,000 km ² north of Toronto and east of Georgian Bay	20 cm	May 5–7, 2013 May 14–17, 2018	Derive image objects in areas of interest for classification; derive features for model development
SCOOP stereo-derived DEM	Same as SCOOP imagery	1 m	May 5–7, 2013	Derive depression and slope data to be used as features for model development
Reference Vernal Pool Dataset (23 sites)	575 ha (25 ha per plot) See Figure 1	NA	April/May, 2016/2017/2019	Train and validate models

water bodies in the forested regions of each plot were mapped.

Datasets

Reference PVPs

To be consistent with the literature (e.g. Brooks et al. 1998; Calhoun et al. 2003; Lathrop et al. 2005), we define vernal pools as temporary to semi-permanent bodies of water that serve as primary breeding habitat for obligate amphibians. Functionally, these can be defined as confined surface depressions with no permanent inflow or outflow. Based on the results of a concurrent study, we knew that at least some of the undocumented wetlands encountered during the surveys supported vernal-pool obligates; however, given the limited time we had to conduct larval surveys during the breeding season, we could not confirm the presence of obligate amphibian breeders in every wetland we encountered. Therefore, in this study, we have designated all undocumented wetlands as PVPs.

We imported the locations and rough boundaries of PVPs identified during the field surveys into ArcGIS Pro 2.5.0 and created a reference dataset by refining the boundaries of each PVP using 20-cm resolution leaf-off color-infrared (CIR) orthoimagery from the South Central Ontario Orthophotography Project (SCOOP; see Table 1). Based on visual interpretation of the SCOOP imagery at each PVP location, we also split each PVP into classes of open water and covered water (water covered by trees or other vegetation). Lastly, we digitized the remaining land cover in the SCOOP imagery into classes of impervious surfaces (e.g. bedrock, roads), shadows, or forest.

Image data sources

The primary sources of data used as input for our machine learning classifiers were the SCOOP products and European Space Agency's (ESA) Sentinel 2 imagery (Table 1). We also used two layers of wetlands and other water bodies created by the Ontario Ministry of Natural Resources and Forestry (OMNRF) to screen out water bodies that had had been previously classified.

SCOOP. SCOOP has been funded through multiple government agencies (federal, provincial, municipal) to provide seamless aerial imagery of south-central Ontario at 5-year intervals (2013, 2018, etc.) and is freely available to all stakeholders and applicable research institutions. The 2013 and 2018 SCOOP products included 20-cm resolution leaf-off CIR orthoimagery and a 2-m resolution, stereoscopically derived Digital Terrain Model (DTM). While we were unable to correct for true reflectance using the available orthoimagery metadata, each dataset was derived from overlapping stereo images to be consistent in tone and appearance. Close inspection of each dataset revealed no discernible differences in the spectral signatures of major land classes within the study region. In addition, the imagery was acquired within a 4-day rainless period for the study region, meaning changes in vegetation and surface wetness within datasets were likely minimal. Using tools in ArcGIS, we derived a Normalized Difference Water Index (NDWI) and slope data from the SCOOP products. We also derived a depression likelihood map using the Stochastic Depression Analysis tool in Whitebox Geospatial Analytical Tools version 3.3 (Lindsay 2016). Stochastic depression analysis accounts for uncertainties in

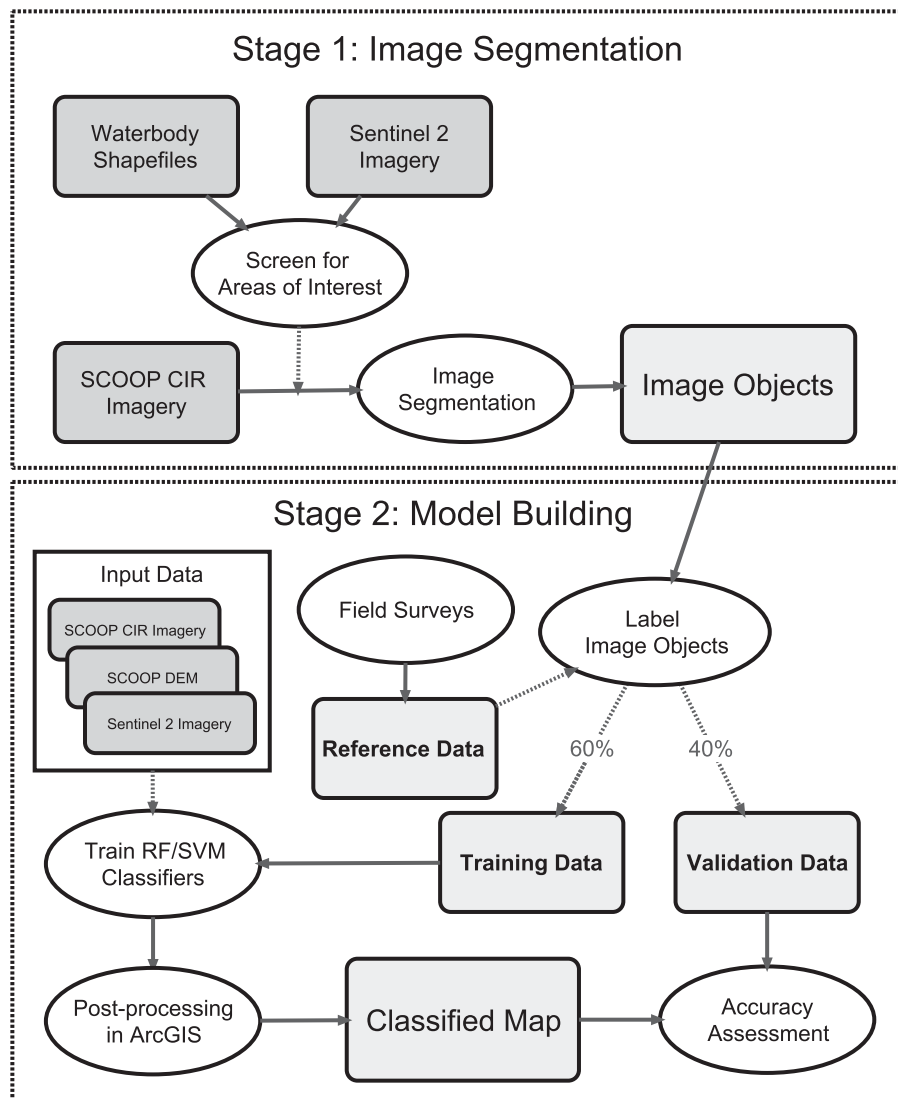


Figure 3. A flowchart depicting the two stages of our model development: stage 1 (top panel) image segmentation of high-resolution leaf-off CIR imagery and stage 2 (bottom panel) model building through training and validation of RF and SVM classifiers using reference data from field surveys. CIR: Color-Infrared; DEM: Digital Elevation Model; RF: Random Forest; SVM: Support Vector Machines; SCOOP: South Central Ontario Orthophotography Project.

DTMs when evaluating the likelihood that a particular geographic area exists as a depression in the landscape (Lindsay 2005). In their approach to map vernal pools in Massachusetts, Wu et al. (2014) found success using stochastic depression analysis to account for uncertainty in LiDAR derived digital elevation models. The SCOOP imagery bands and the SCOOP-derived products were used as inputs for the machine learning classifiers. The SCOOP imagery bands were also used during the segmentation procedure to create image objects.

Sentinel. We downloaded Sentinel 2 Level 1C products from the U.S. Geological Survey's (USGS) EarthExplorer portal in mid-spring for dates with low cloud cover that coincided with the field surveys

(April 27, 2016; May 7, 2018; May 5, 2019; see Table 1). Since most of the snow had melted by late April, we have assumed that vernal pools in these satellite images were maximally inundated. We preprocessed the image in ESA's Sentinel Application Platform version 7.0 (SNAP) using the Sen2Cor processor version 280 to create Level 2A terrain-corrected, bottom-of-atmosphere reflectance products. The Scene Classification map created as part of Sen2Cor processing was used to mask out clouds and cloud shadows from the corrected images. While Sentinel 2 has bands with resolutions of 10, 20, and 60 m, we were interested in the 10 m bands (Blue, Green, Red, and NIR) for the purposes of detecting small forested vernal pools. The corrected bands were averaged across years to create a single multiband

Table 2. Features extracted for each object following image segmentation.

Data	Object features
SCOOP imagery	RGB/NIR band means and standard deviations for 2013 and 2018 imagery Mean Brightness (mean of all bands) for 2013 and 2018 Means of averaged 2013 and 2018 RGB/NIR bands NDWI mean and standard deviation GLCM and GLDV statistics for NIR bands: angular second moment, contrast, correlation, dissimilarity, entropy, homogeneity, mean, standard deviation
SCOOP DTM	DTM standard deviation Mean and standard deviation of slope and depression likelihood
Sentinel 2 imagery	RGB/NIR band means
OMNRF Wetlands/Waterbodies	Existence of neighboring waterbodies (binary)
Object Shape	Area, asymmetry, border index, border length, compactness, density, elliptic fit, length, length/thickness, length/width, roundness, shape index

DTM: Digital Terrain Model; GLCM: Gray Level Cooccurrence Matrix; GLDV: Gray Level Difference Vector; NIR: Near Infrared; NDWI: Normalized Difference Water Index; OMNRF: Ontario Ministry of Natural Resources and Forestry; RGB: Red Green Blue.

image and the NIR band was used to screen for pixels likely to be inundated based on a threshold of <0.195 reflectance units. We determined this threshold by averaging reflectance units of pixels along the edges of known wet forest locations. The averaged Sentinel 2 bands were also used as inputs for the machine learning classifiers.

Model development for classification of PVPs

Image segmentation

Our object-based machine learning approach to classify vernal pools was broken down into two stages (Figure 3). The first stage involved segmenting our high-resolution SCOOP imagery using Trimble Geospatial's object-based image analysis platform, eCognition version 9.2. Areas of interest were first extracted for each plot with Sentinel 2 thresholding and by masking previously classified water bodies. Then we performed multiresolution segmentation on these areas of interest using the two sets of imagery bands to create image objects. We assigned a weight of 1 to each of the RGB bands and 2 to the NIR bands because the NIR band exhibits high contrast between water and non-water features. The multiresolution segmentation algorithm has three parameters that control the shape and position of image objects: scale, shape, and compactness. The scale parameter controls the amount of spectral variation within image objects, which relates to object size. The shape parameter controls the degree to which object shape and color factor into segmentation. The compactness parameter controls the weighting between the compactness and smoothness of an object's shape. We selected a range of realistic values for each parameter (Scale: 10–1000; Shape and Compactness: 0.1–0.9) and tested each combination on three test study plots by visually inspecting how well the resultant objects overlapped with the class boundaries on the reference

dataset. Using this process, we determined an optimal parameter combination of 100, 0.25, and 0.25 for scale, shape, and compactness, respectively.

To reduce the number of image objects representing non-water bodies, we applied a spectral difference algorithm on the objects created through segmentation. The spectral difference algorithm merges neighboring objects that have a difference in spectral means below a given threshold. We weighted the NIR bands three times higher than the other bands to make it difficult for water bodies to be merged with nonwater bodies. We used a qualitative approach to assign a threshold for the spectral difference algorithm. We started with a threshold of 2 and raised it until the algorithm started to merge water bodies with non-water bodies. Using this approach, we selected a threshold of 8 digital number units.

Image objects were exported in shapefile format (.shp) with feature attributes derived from the SCOOP products, the Sentinel 2 bands, the OMNRF waterbodies, and the shapes of the objects (Table 2). In addition to deriving means and standard deviations of our datasets, we derived Haralick texture features from the Gray Level Cooccurrence Matrix (GLCM) and the Gray Level Difference Vector (GLDV) of the mean NIR bands using omnidirectional pixel-pair sampling. These metrics describe the texture of each image object based on the NIR bands and are useful in other wetland-based classification studies (Chatziantoniou et al. 2017; Ma et al. 2015).

Model building

The second stage of our classification approach involved the evaluation of machine learning classifiers, Random Forest (RF) and SVM, for mapping PVPs using the object features extracted from image segmentation (Table 2). Our modeling framework was broken down into five steps: (1) assigning class labels to image objects, (2) creating training and validation

datasets, (3) selecting features, (4) training models, and (5) post-classification adjustments. Class labels assignment and post-classification adjustments were completed in ArcGIS Pro, while the rest of the modeling framework was performed in R, version 3.6.2.

For the first step, we started by overlaying the classified reference dataset shapefile on the image object shapefile to calculate class percentages for each object. We then labeled each object with their majority class. In order to ensure strong class representation in our training data, we subset the image objects using a threshold of $>60\%$ overlap with the majority class.

To separate our image objects into training and validation datasets, we iterated through random assignments of study plots to either the training or validation datasets (60% to training and 40% to validation) until the class distributions for the training and validation datasets did not differ by more than 10% from the class distributions in the complete dataset. We also made sure that the plots used to refine the segmentation parameters were part of the training dataset. While this approach may lead to autocorrelation between the training and validation datasets, we decided it was necessary to ensure sufficient representation of the PVP objects for each dataset.

The feature selection step of our model framework was used to select a subset of relevant features for model training because some features can be either redundant or irrelevant to classification and can lead to poor accuracy. Feature selection techniques help mitigate these problems in addition to problems associated with overfitting and unacceptably long computation time. This is especially important for OBIA where segmentation procedures lead to significantly more features than pixel-based methods. To select the feature subset for model training, we applied Recursive Feature Elimination (RFE) to the training dataset using the caret package in R (Kuhn 2019). RFE is a backward feature elimination technique and works by fitting successive models and removing the weakest features until a specified number of features are left. We used random forest models to run RFE and the mean decrease in accuracy to determine feature importance. This measure determines feature importance by finding the difference in prediction error between models with and without each feature. To select an optimal subset size, we used K-fold cross-validation (CV) for a range of subset sizes (8, 16, 24, 32, 40, and 57 features). CV reduces problems associated with overfitting by splitting the training data into K groups and running K RFE models, such that for each model, one of the K groups is reserved

as a test set and the remaining K-1 groups are used to train the model. We chose 10 folds for our study, as this value has been recommended in the literature (Kuhn and Johnson 2013). Average model performance across the 10 repeated models can then be compared for the different subset sizes to determine the optimal subset of features.

Once we decided on a subset of features, we used the train function in the caret package to optimize the machine learning classifiers for our training dataset. Each machine learning classifier has one or more parameters that can be optimized for model performance. For RF, the optimization parameters the number of features that are randomly selected for splitting at each node in the classification tree (mtry), and the number of individual classification trees to run for the model (ntree). For SVM, the optimization parameters depend on the type of kernel used. We used the radial basis function as the kernel for our classifier as it has yielded strong results in other remote sensing applications (Kavzoglu and Colkesen 2009). SVM with a radial basis function has two optimization parameters: sigma, which describes the influence of individual support vectors; and cost, which controls the penalty for misclassified points. Both parameters impact the tradeoff between model simplicity and misclassification. For each classifier, we selected a range of possible values for each parameter and used repeated CV to estimate performance metrics for each unique parameterization. Repeated CV accounts for potential variability in model performance metrics across different splits of the data by averaging over multiple CV procedures. We used 10 folds for each CV and took an average after the CV procedure was repeated 10 times. Because our classes were highly imbalanced (there were 10–100 times more objects in the forest class than in other classes), we also incorporated down-sampling into the model training procedure. The main problem with class imbalances is that the majority class is the main driver of model fit, meaning infrequent classes can be underrepresented in the final model. Down-sampling mitigates this by randomly selecting a subset of each class such that every class has the same number of observations. Down-sampling was applied after each of the $N \times K$ sub-sampling procedures.

Since our goal was to inventory all PVP locations, we focused on the open-water class rather than all classes to assess the performance of each model parameterization. We used an F-Score as our performance metric, which is a weighted average of precision and recall, and is calculated according to the following

equations:

$$\text{precision} = \frac{\# \text{ true positives}}{\# \text{ true positives} + \# \text{ false positives}}$$

$$\text{recall} = \frac{\# \text{ true positives}}{\# \text{ true positives} + \# \text{ false negatives}}$$

$$F_{\beta} = (1 + \beta^2) \frac{\text{precision} \times \text{recall}}{(\beta^2 \times \text{precision}) + \text{recall}}$$

Where β is the weight of the *F*-Score. When $\beta > 1$, recall is weighted higher than precision, and when $\beta < 1$, precision is weighted higher than recall. For this study, we were more interested in minimizing false negatives over false positives because false positives are easier to rectify in the field. As such, we chose $\beta = 2$ to favor false negatives. The model parameterization with the highest *F*-Score was used as the final model for each classifier.

Once each machine learning model was trained, we exported the objects with their predicted classes to ArcGIS Pro and performed a final set of post-classification adjustments based on spatial relationships. First, we merged neighboring objects with the same class together to create seamless objects. To account for boundary inaccuracies of previously classified large waterbodies, we applied a 10-m buffer around these and labeled all open-water or covered-water objects overlapping this buffer as “OMNRFwater”. We assigned any impervious surface objects that overlapped with an OMNRF road shapefile to a “road” class. To minimize commission errors resulting from shadows on road being misclassified as open water due to similar spectral properties, we assigned any open-water objects sharing a border with a road to the “shadow” class. We considered all open-water objects and any covered-water objects that bordered open-water objects as part of the “PVP” class. Given that all the PVPs we surveyed in the field were separated by greater than 20 m distance from each other, we merged PVPs occurring within 20 m into a single PVP object. All other covered-water objects that did not share a border with open-water objects were assigned to the “forest” class.

Accuracy analysis

We applied the modeling framework to the validation dataset and completed the same post-classification adjustments used on the training dataset to produce a classified dataset for unbiased accuracy analysis. Since our primary interest was the location of vernal pools, we used an object-based metric of success defined by if the location of PVPs in our classified dataset

overlapped those in our reference dataset. As such, true positives were classified as PVPs that overlapped with reference PVPs, false positives were classified PVPs that did not exist as PVPs in the reference dataset, and false negatives were reference PVPs that were not mapped in the classified dataset. While we considered any overlap between classified and reference objects to represent true positives, we recognize that a more conservative overlap criterion would reduce the estimated accuracy of the models. We were less concerned with PVP shape and size compared to PVP location, so this criterion was acceptable for our purposes. To compare the RF and SVM classifiers, we used another *F*-Score with a $\beta = 2$ to put more emphasis on false negatives.

To maximize the accuracy of our reference dataset, we included all water bodies encountered through field sampling, and this included extremely small pools ($< 50 \text{ m}^2$) that tended to dry out before obligate amphibian larvae could develop. Since these pools were less frequently associated with obligate amphibians and were considerably more difficult to identify, we decided to only include PVPs $> 50 \text{ m}^2$ to calculate producer's accuracy. We also investigated possible effect of pool size and distance from roads on true positives, false positives, and false negatives in our classified results. Due to differences in the average size of PVP objects between the reference and classified datasets, we separately compared the median areas of true positives to false positives and of true positives to false negatives using the reference and classified datasets, respectively. We used a similar approach when comparing the percentage of PVP objects within 100 m of a road.

Results

Within the 23 forested plots (each $500 \times 500 \text{ m}$) in southeastern Georgian Bay, we encountered 133 PVPs ($> 50 \text{ m}^2$) that had not been mapped by the OMNRF as either water body or wetland. These hitherto undocumented wetlands ranged from small pools with open water and sparse vegetation (typically $< 500 \text{ m}^2$) to large wetlands dominated by emergent vegetation (typically $> 500 \text{ m}^2$), although the median size was relatively small (222 m^2). The large vegetated wetlands ($> 500 \text{ m}^2$) we encountered would not be typically designated as vernal pools in the literature, but we found that the edges of these wetlands often contained temporary pools of water that provided similar habitat as traditional vernal pools. In fact, many of these edge

Table 3. Features selected for model training in order of estimated importance (Imp).

Object features	Imp	Object features	Imp	Object features	Imp
Mean NDWI (2013)	10.4	SD Green (2013)	6.5	Mean Red (2018)	4.7
Mean Green (Sentinel)	9.9	Mean Blue (average of 2013 and 2018)	6.4	Mean Slope	4.1
Mean Red (Sentinel)	9.3	Mean NIR (2018)	6.3	SD Depression	3.3
Mean NIR (Sentinel)	9.2	Mean Blue (2013)	6.3	SD Blue (2013)	3.2
Mean NIR (average of 2013 and 2018)	8.9	Mean Red (2013)	5.6	SD NIR (2018)	3.2
Mean Blue (Sentinel)	8.5	Mean Green (2013)	5.4	GLCM Angular Second Moment	3.1
Brightness	7.2	SD Slope	5.2	Border Index	3.0
Mean NIR (2013)	7.1	Mean Green (2018)	5.0	SD NDWI (2013)	3.0
Mean Depression Likelihood	7.1	Mean Blue (2018)	4.9	Shape Index	2.9
Mean Green (average of 2013 and 2018)	6.7	Existence of OMNRF waterbodies as neighbor	4.8	GLCM Entropy	2.9
Mean Red (average of 2013 and 2018)	6.5			SD NIR (2013)	2.9

The years in brackets (2013 or 2018) correspond to the imagery dataset year for the South Central Orthophotography Project. GLCM: Gray Level Cooccurrence Matrix; NDWI: Normalized Difference Water Index; NIR: Near Infrared; SD: standard deviation; OMNRF: Ontario Ministry of Natural Resources and Forestry.

pools were opportunistically observed to contain eggs of vernal pool obligate amphibians.

Although our use of the Sentinel band 8 threshold and the OMNRF wetlands/waterbodies resulted in omission of two reference PVPs, this procedure reduced the area for analysis by 75%, and saved a lot of time and processing power. In trials without the use of Sentinel imagery to screen for potentially inundated areas, we found unacceptably high errors of commission that would have falsely indicated an abundance of vernal pool habitat.

The segmentation procedure created 13,106 objects with a mean size of 178 m². Of these objects, 95% overlapped a reference layer class by more than 60% and were labeled with this class. We used 7518 objects in 14 training plots to train the machine learning classifiers. Most of these objects were labeled as forest (84%), while a smaller portion were labeled as covered water (7%), impervious surfaces (5%), open water (2.5%), and shadows (1.5%).

The RFE procedure selected a subset of 32 unique object features that were deemed important for model training (Table 3). Roughly 60% of the selected features were derived from means and standard deviations of SCOOP imagery bands or band derivatives. Of the remaining features, four were derived from Sentinel imagery bands, four from the SCOOP DTM derivatives, two from the GLCM and GLDV, two from the object shape, and one from the existence of neighboring OMNRF waterbodies.

We used cross-validation to select for the optimal model parameterization for the RF and SVM machine learning classifiers. The optimal parameterization for the RF model used an mtry of 2, an ntree of 200, and achieved cross-validated F-Score of 0.65 (precision = 0.44, recall = 0.75). The optimal parameterization for the SVM model used sigma of 0.05 and a cost of 1. This parameterization yielded an F-Score of 0.58 (precision = 0.39, recall = 0.68). It is worth noting that using

a custom F-Score that puts more weight on the class of interest resulted in different parameterizations for each model when compared to using the default accuracy metrics. When we used more common accuracy metrics of Overall Accuracy and Kappa Score, we ended up with lower final accuracies for our vernal pool classification. Overall Accuracy and Kappa Score weigh classes evenly, so, while the classifier may perform better overall, most of the resultant classes are not relevant for the accuracy of vernal pool delineation.

The trained RF and SVM models were applied to the objects within the validation plots to produce 5129 classified objects for each classifier. Both classifiers produced similar proportions of classes: 5–6% open water, 5–9% shadows, 7–9% impervious surfaces, 22% covered water, and 57–58% forest. The increased proportion of open-water and covered-water classes compared to the reference dataset was mainly a result of extensions of the OMNRF waterbodies that were missed during the digitization of the reference dataset. Similarly, the increased proportion of shadows in the training dataset compared to the reference dataset was because the lighter-colored shadows in the SCOOP imagery had not been identified as such in the reference dataset. The majority of the objects classified as open water were adjacent to other water objects: open water, covered water, or OMNRF waterbodies (90 and 77% for RF and SVM, respectively). When using the post-classification procedure to group these spatially associated objects, we obtained 59 objects classified as PVPs for the RF classifier and 44 for the SVM classifier (Figure 4). The median size of the PVP objects classified by RF was only slightly larger than that in the reference dataset (285 vs. 222 m², respectively), whereas those classified by SVM were twice as large (442 vs. 222 m², respectively).

We assessed the accuracy of the PVP objects from the post-classification procedure using the F-Score, a weighted average of precision (user's accuracy) and

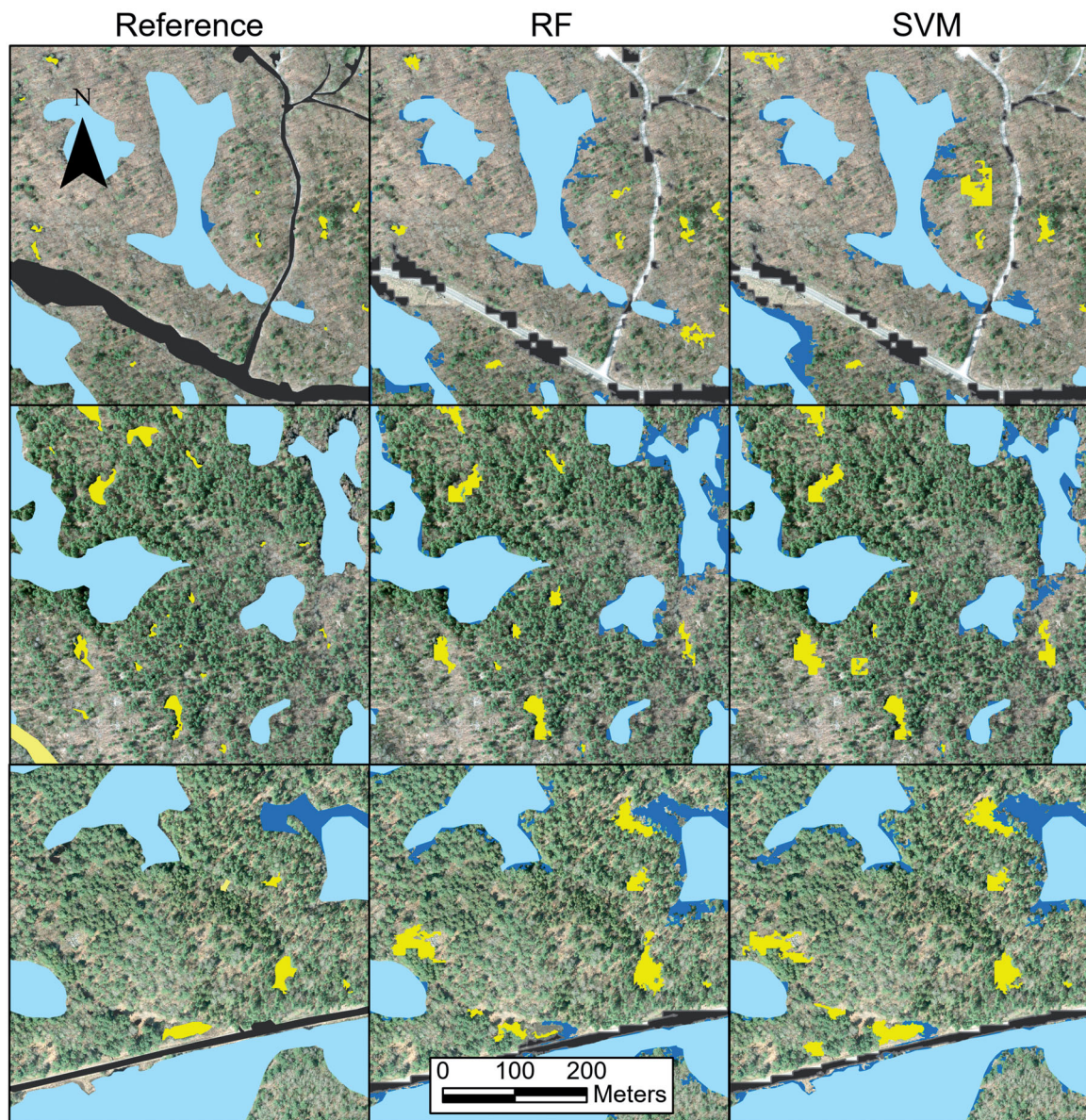


Figure 4. Comparison of classification results from each model (RF: random forest; SVM: support vector machines) with the reference dataset for three sites: GB2 plot 2 (top), GB3 plot 1 (middle), and GB6 plot 4 (bottom). The light blue polygons represent land previously identified as waterbodies by the Ontario Ministry of Natural Resources and Forestry (OMNRF). The black polygons represent areas classified as roads. The dark blue polygons represent areas classified as being “OMNRFwater” (i.e. missed portions of the OMNRF identified waterbodies). The yellow polygons represent areas classified as “PVP” (potential vernal pools). Basemap source: Ontario Ministry of Natural Resources and Forestry.

Table 4. Comparison of accuracy metrics for each model.

Model	Random forest	Support vector machines
User's accuracy	78.0%	84.1%
Producer's Accuracy	85.4%	79.1%
F-Score ($\beta = 2$)	0.83	0.81

Accuracy was assessed based on the proportion of overlapping potential vernal pool polygons between the reference and classified datasets. User's accuracy was calculated based on 59 classified potential vernal pool objects (PVP) objects for the Random Forest model and 44 classified PVP objects for the Support Vector Machine model. Producer's accuracy was calculated based on 48 reference PVP objects for both models. F-score was calculated using a β value of 2 to place a higher emphasis on minimizing errors of omission.

recall (producer's accuracy). The F-Score we used in this study placed a higher weight on false positives, meaning that producer's accuracy had a stronger influence than user's accuracy. There appeared to be a direct tradeoff between producer's and user's accuracies between the two classifiers. Whereas the RF classifier had higher producer's accuracies, the SVM classifier had comparatively higher user's accuracies (Table 4). Since producer's accuracy was weighted higher, the RF classifier produced higher F-Scores when compared to the SVM classifier (Table 4).

Table 5. Comparison of potential vernal pool (PVP) polygon size and percentage found within 100 m of roads for reference and classified datasets using the random forest model.

	Reference PVPs		Classified PVPs	
	Mapped (<i>N</i> = 41)	Omitted (<i>N</i> = 7)	True positives (<i>N</i> = 46)	False positives (<i>N</i> = 13)
Median size (m ²)	217	93	369	82
Within 100 m of road (%)	24	14	28	38

Mapped reference PVPs were those correctly classified by the model, while omitted reference PVPs were those missed by the model.

Consequently, our optimal model using the RF classifier had an omission rate of 15% and a commission rate of 23% for reference PVPs.

Approximately 85% of the correctly classified PVP objects overlapped PVP objects from the reference dataset by more than 50%. The remaining 15% of correctly classified PVP objects overlapped the reference dataset by more than 20% but less than 50%. These PVPs tended to be highly vegetated with few areas of open water. The median size of PVPs that were correctly mapped in both the reference and classified datasets were larger than those that had been missed or were the result of commission error (Table 5). Another factor that may have affected mapping accuracy was difficulty in distinguishing between PVPs and the shadow class due to spectral confusion. This was supported by the fact that only 24% of the PVPs in the reference dataset occurred within 100 m of roads, while 38% of false positives occurred within this buffer (Table 5). Closer inspection of SCOOP imagery confirmed that false positives were always associated with dark shadows, which were especially common near roadways and on exposed bedrock. False-negative PVPs included small PVPs (<100 m²), those with high canopy cover, and those on slopes or exposed bedrock with small drainage basins. These PVPs were difficult to distinguish from the shadow class.

Discussion

Remote sensing approaches for mapping small ephemeral wetlands have been prevalent during the last decade (Bourgeau-Chavez et al. 2016; Carpenter et al. 2011; Cormier et al. 2013; DiBello et al. 2016; Julian et al. 2009; Leonard et al. 2012; Riley et al. 2017; Wu et al. 2014). This study contributes to this growing knowledge base by combining documented wetland mapping techniques to develop an efficient classifier for vernal pools in a remote area of Ontario. We confirmed that groups of pixels representing vernal pools in high-resolution leaf-off CIR imagery can be separated from surrounding land-use with OBIA. Further, we found that machine learning was able to classify objects from OBIA based on the spectral, texture,

shape, and neighborhood characteristics of each object. Our object-based machine learning approach was able to accurately predict the locations of PVPs with a minimum size threshold of 50 m², with a corresponding producer's accuracy of 85% and user's accuracy of 77%. It is noteworthy that past studies that have achieved similar or better results for forested wetlands of comparable size required the use of LiDAR -derived data products, which are expensive and not yet available for remote regions in Ontario (Leonard et al. 2012; Riley et al. 2017; Wu et al. 2014; but see Bourgeau-Chavez et al. 2016).

This study also highlights the shortcomings of previous wetland mapping projects in the province. The wetland and waterbody datasets from the OMNRF accounted for 116 individual wetlands that intersected the 23 study plots. Our field surveys uncovered an additional 133 undocumented wetlands, more than doubling the estimate of wetland density for the region. While the provincial wetland and waterbody datasets remain very important for planning and watershed management, our study can supplement these data to provide an even stronger understanding of the water resources in this region of Ontario.

The RF and SVM classifiers performed similarly well in our study, though RF had a higher user's accuracy and tended to produce PVPs of more comparable size to the reference data. Neither classifier assumes any particular distribution of data and both are robust to noise and errors (Ma et al. 2017a). Studies that have reported RF outperforming SVM argue that SVM is more prone to overfitting the data because it is trained on the entire dataset whereas RF is trained on random subsets for each decision tree (Amani et al. 2017; Tian et al. 2016). Our use of repeated CV to subset the data during model training likely reduced the discrepancies between the RF and SVM classifiers with respect to overfitting the data. Though we did not compare computation time in our study, RF has generally been found to be faster when compared to SVM, thus making RF the better option when the two methods produce similar accuracies.

While our classification produced acceptable results for our purposes, we recognize that there are other

options for model optimization that we did not explore. For example, we used a single feature selection algorithm and measure of importance to decide on an optimum feature subset. Given the diversity of feature selection methods available for remote sensing applications (e.g. Ma et al. 2017a), it is possible that different feature selection algorithms and importance measures could provide a more accurate prediction of the optimal feature set (Jović et al. 2015; Ma et al. 2017b). We also relied on a down-sampling approach to account for the issue of class imbalances. Though down-sampling is simple to implement, it can miss important discriminatory characteristics of the majority class and reduce the likelihood of capturing class variance, leading to potentially large inaccuracies in the model (He and Garcia 2009). Other resampling methods, such as up-sampling and the synthetic minority over-sampling technique, manipulate the data in different ways and may allow for a more accurate representation of the PVP classes in the model (Chawla et al. 2002; Douzas et al. 2019; Maxwell et al. 2018). Cost-sensitive measures, which assign higher costs to misclassifications of the minority classes compared to those of the majority classes, are also common approaches for dealing with class imbalances and avoid resampling the data (He and Garcia 2009). While these alternative approaches also come with their own drawbacks, it is certainly possible that a comparison of approaches could yield a more accurate classification of vernal pools.

Our classifier had trouble differentiating between small pools and shadows on impervious surfaces. Conifer shadows on bedrock or roadsides shared similar spectral properties with areas of inundation and accounted for all errors of commission in our models. Similarly, small pools or pools with high canopy cover were often misclassified as shadows. Past vernal pool detection studies have had similar trouble differentiating small pools from shadows (Cormier et al. 2013; Faccio et al. 2013), though the inclusion of LiDAR-derived products has been found to reduce these errors (Leonard et al. 2012; Reutebuch et al. 2003). A smaller proportion of reference pools were missed because of the Sentinel 2 screening process. These pools were typically perched on exposed bedrock and had small drainage basins that accounted for only a fraction of the Sentinel 2 pixel size. We found these pools to be less prevalent across our study region and they only accounted for a small fraction of the false negatives in our accuracy analysis.

We focused our mapping efforts on the coast of southeastern Georgian Bay because it is a highly

coveted area for current and future development. Our approach should be informative for our region of interest as the topography and land cover are relatively homogenous (Crins et al. 2009). If this approach were to be applied over the larger SCOOP extent, which stretches 150 km to the south and east of our study region (Figure 1), additional samples would be required. Our study sites are clustered and localized for our specific region, so it is unlikely that we have accounted for the full variation in topography and land cover encompassed by the SCOOP products. Similarly, it may be possible to obtain comparable mapping accuracies for regions covered by different Ontario Orthoimagery Projects (OOP), but models would need to be retrained with new field data. The suite of OOPs have differences in spectral characteristics stemming from the time of year when images were acquired, weather conditions before and during image capture, and the camera system used to take the images (Ontario Ministry of Natural Resources and Forestry (OMNRF) 2020). The accuracy of these new classifiers may be improved or reduced due to differences in landscape characteristics, such as topography and forest composition (Lathrop et al. 2005), or differences in the characteristics of the OOP, such as image quality and number of years of imagery.

Though the orthoimagery projects of Ontario were not intended to be used for supervised image classification, we believe they are a useful tool for small-scale mapping projects especially when combined with OBIA. Vernal pools are small, obscure, and critically understudied in Ontario. They provide essential habitat for amphibian species, such as mole salamanders (*Ambystoma jeffersonianum*, *A. laterale*, *A. maculatum*) and wood frogs (*Lithobates sylvaticus*), and act as important secondary habitat and stopover sites for species at risk, including Blanding's turtles (*Emydoidea blandingii*; Markle and Chow-Fraser 2014). Vernal pools also provide many ecosystem services including water retention, energy transfer, and nutrient cycling (Hunter 2007; Leibowitz 2003). The conservation of these ecosystems will be important for Ontario, especially in regions that are under high development pressure, such as southeastern Georgian Bay. The classification models from this study should be used to identify vernal pool hotspots and narrow down locations to conduct ground surveys for verification of vernal pools. To verify the locations of vernal pools based on the classified maps, we suggest that surveyors confirm not only the presence of water, but also the presence of obligate amphibian breeders. This would involve either egg or

larvae surveys, depending on the time of year. Though Ontario does not have a strict definition of vernal pools, these constraints are consistent with other N. American jurisdictions that have existing vernal pool mapping programs (Brooks et al. 1998; DiBello et al. 2016; Faccio et al. 2013). While field verification is certainly feasible for projects focused on small areas of interest, the detailed and time-consuming nature of the field work may make this methodology infeasible for large areas of interest.

To date, there are no comprehensive databases of vernal pools for forests of southeastern Georgian Bay or any forested region in Ontario. Knowledge of vernal pool distributions would fill a notable gap in understanding the importance of habitat connectivity for wildlife that are associated with wetland networks. This knowledge will also be important for deciphering the potential impacts of climate change and land-use changes on water resources, including earlier drying and loss of landscape connectivity (Brooks 2009). Although inclusion of high-resolution LiDAR and RADAR data would no doubt improve our mapping, this technology is too expensive to be widely available, and the need for information on vernal pool distribution is too great to hold out for these data.

Conclusion

The study presented here showed that an OBIA approach using high-resolution multispectral imagery and machine learning classification is a promising approach for the detection of PVPs in heavily forested regions of central Ontario. Vernal pools are often overlooked in regional wetland mapping projects due to their small size and the obstruction from the forest canopy. The use of image segmentation to identify homogenous regions of sub-meter-resolution aerial imagery allowed for the detection of forested vernal pools down to a visible surface area of 50 m². Our study found that the RF classifier marginally outperformed the SVM classifier, providing final producer's and user's accuracies of 85 and 79%, respectively.

Errors encountered in this study were the result of misclassifications between small pools and shadows from coniferous trees. It is unlikely that an approach relying exclusively on multispectral imagery can eliminate these types of errors. Once high-resolution LiDAR and/or RADAR become available for these remote regions, the accuracy and precision of this approach will likely improve. In the meantime, this approach provides an efficient method to identify PVPs, thus greatly reducing the time, financial

commitment and human resources needed to improve upon local-scale databases of wetland resources.

Acknowledgements

We would like to thank all individuals involved in field surveys for this study, including James Marcaccio, J. Daniel Weller, Chantel Markle, Oliver Wearing, Morgan Piczak, Jonah Lehman, and Cameron Brown. We would like to thank Jean DeMarco and Ralph and Caroline Grose for hosting field crews at their cottages during our surveys. We would also like to thank Sarah Walton-Rabideau for help with the production of verification maps for early iterations of the model. Funding for this project was provided by the Natural Sciences and Engineering Research Council of Canada in the form of a Discovery Grant to PC-F and a PGS-D to NL, and the Boreal Water Futures project, a project of the Global Water Futures Program funded by the Canada First Research Excellence Fund. We greatly appreciate the suggestions of two anonymous reviewers.

Disclosure statement

No potential conflict of interest was reported by the author(s).

ORCID

Nick Luymes  <http://orcid.org/0000-0003-0290-6028>

Patricia Chow-Fraser  <http://orcid.org/0000-0002-0416-7196>

References

- Amani, M., Salehi, B., Mahdavi, S., Granger, J.E., Brisco, B., and Hanson, A. 2017. "Wetland classification using multi-source and multi-temporal optical remote sensing data in Newfoundland and Labrador, Canada." *Canadian Journal of Remote Sensing*, Vol. 43(No. 4): pp. 360–373. doi:10.1080/07038992.2017.1346468.
- Baldwin, R.F., and deMaynadier, P.G. 2009. "Assessing threats to pool-breeding amphibian habitat in an urbanizing landscape." *Biological Conservation*, Vol. 142(No. 8): pp. 1628–1638. doi:10.1016/j.biocon.2009.02.039.
- Blaschke, T. 2010. "Object based image analysis for remote sensing." *ISPRS Journal of Photogrammetry and Remote Sensing*, Vol. 65(No. 1): pp. 2–16. doi:10.1016/j.isprsjrs.2009.06.004.
- Bourgeau-Chavez, L., Lee, Y., Battaglia, M., Endres, S., Laubach, Z., and Scarbrough, K. 2016. "Identification of woodland vernal pools with seasonal change PALSAR data for habitat conservation." *Remote Sensing*, Vol. 8 (No. 6): pp. 490. doi:10.3390/rs8060490.
- Brooks, R.T. 2009. "Potential impacts of global climate change on the hydrology and ecology of ephemeral freshwater systems of the forests of the Northeastern United States." *Climatic Change*, Vol. 95(No. 3–4): pp. 469–483. doi:10.1007/s10584-008-9531-9.

- Brooks, R.T., Stone, J., and Lyons, P. 1998. "An inventory of seasonal forest ponds on the Quabbin Reservoir Watershed." *Northeastern Naturalist*, Vol. 5(No. 3): pp. 219. doi:10.2307/3858622.
- Calhoun, A.J.K., Mushet, D.M., Bell, K.P., Boix, D., Fitzsimons, J.A., and Isselin-Nondedeu, F. 2017. "Temporary Wetlands: Challenges and Solutions to Conserving a 'disappearing' Ecosystem." *Biological Conservation*, Vol. 211 (July): pp. 3–11. doi:10.1016/j.biocon.2016.11.024.
- Calhoun, A.J.K., Walls, T.E., Stockwell, S.S., and Mccollough, M. 2003. "Evaluating vernal pools as a basis for conservation strategies: A Maine case study." *Wetlands*, Vol. 23(No. 1): pp. 70–81. Springer. doi:10.1672/0277-5212(2003)023.[0070:EVPAAB]2.0.CO;2.
- Carpenter, L., Stone, J., and Griffin, C.R. 2011. "Accuracy of Aerial Photography for Locating Seasonal (Vernal) Pools in Massachusetts." *Wetlands*, Vol. 31(No. 3): pp. 573–581. doi:10.1007/s13157-011-0169-4.
- Chatziantoniou, A., Psomiadis, E., and Petropoulos, G. 2017. "Co-orbital sentinel 1 and 2 for LULC mapping with emphasis on wetlands in a mediterranean setting based on machine learning." *Remote Sensing*, Vol. 9(No. 12): pp. 1259. doi:10.3390/rs9121259.
- Chawla, N.V., Bowyer, K.W., Hall, L.O., and Kegelmeyer, W.P. 2002. "SMOTE: Synthetic minority over-sampling technique." *Journal of Artificial Intelligence Research*, Vol. 16(June): pp. 321–357. doi:10.1613/jair.953.
- Cormier, T.A., Congalton, R.G., and Babbitt, K.J. 2013. "Spatio-statistical predictions of vernal pool locations in Massachusetts." *Photogrammetric Engineering & Remote Sensing*, Vol. 79(No. 1): 25–35. doi:10.14358/PERS.79.1.25.
- Crins, W. J., Gray, P.A., Uhlig, P.W.C., and Wester, M.C. 2009. *The Ecosystems of Ontario, Part 1: Ecozones and Ecoregions*. Sault Ste. Marie: Ontario Ministry of Natural Resources.
- DiBello, F.J., Calhoun, A.J.K., Morgan, D.E., and Shearin, A.F. 2016. "Efficiency and detection accuracy using print and digital stereo aerial photography for remotely mapping vernal pools in new england landscapes." *Wetlands*, Vol. 36(No. 3): pp. 505–514. doi:10.1007/s13157-016-0759-2.
- Douzas, G., Bacao, F., Fonseca, J., and Khudinyan, M. 2019. "Imbalanced learning in land cover classification: Improving minority classes' prediction accuracy using the geometric SMOTE algorithm." *Remote Sensing*, Vol. 11(No. 24): pp. 3040. doi:10.3390/rs11243040.
- Dronova, I. 2015. "Object-based image analysis in wetland research: A review." *Remote Sensing*, Vol. 7(No. 5): pp. 6380–6413. doi:10.3390/rs70506380.
- Evans, J.P., Cecala, K.K., Scheffers, B.R., Oldfield, C.A., Hollingshead, N.A., Haskell, D.G., and McKenzie, B.A. 2017. "Widespread degradation of a vernal pool network in the Southeastern United States: Challenges to current and future management." *Wetlands*, Vol. 37(No. 6): pp. 1093–1103. doi:10.1007/s13157-017-0943-z.
- Faccio, S.D., Lew-Smith, M., and Worthley, A. 2013. *Vermont vernal pool mapping project: Final report to the natural heritage information project of the Vermont Department of Fish and Wildlife*. Huntington: Arrowwood Environmental.
- Fu, B., Wang, Y., Campbell, A., Li, Y., Zhang, B., Yin, S., Xing, Z., and Jin, X. 2017. "Comparison of object-based and pixel-based random forest algorithm for wetland vegetation mapping using high spatial resolution GF-1 and SAR data." *Ecological Indicators*, Vol. 73: pp. 105–117. doi:10.1016/j.ecolind.2016.09.029.
- Grenier, M., Labrecque, S., Garneau, M., and Tremblay, A. 2008. "Object-based classification of a SPOT-4 image for mapping wetlands in the context of greenhouse gases emissions: The case of the Eastmain region." *Canadian Journal of Remote Sensing*, Vol. 34(No. sup2): pp. S398–S413. doi:10.5589/m08-049.
- Harken, J., and Sugumaran, R. 2005. "Classification of Iowa wetlands using an airborne hyperspectral image: A comparison of the spectral angle mapper classifier and an object-oriented approach." *Canadian Journal of Remote Sensing*, Vol. 31(No. 2): pp. 167–174. doi:10.5589/m05-003.
- He, H., and Garcia, E.A. 2009. "Learning from imbalanced data." *IEEE Transactions on Knowledge and Data Engineering*, Vol. 21(No. 9): 1263–1284. doi:10.1109/TKDE.2008.239.
- Hunter, M. L. 2007. "Valuing and conserving vernal pools as small-scale ecosystems." In *Science and Conservation of Vernal Pools in Northeastern North America*, edited by A.J.K. Calhoun and P.G. Demaynadier, 1–10. Boca Raton, FL: CRC Press.
- Jansujwicz, J.S., Calhoun, A.J.K., and Lilieholm, R.J. 2013. "The Maine vernal pool mapping and assessment program: engaging municipal officials and private landowners in community-based citizen science." *Environmental Management*, Vol. 52(No. 6): pp. 1369–1385. doi:10.1007/s00267-013-0168-8.
- Jović, A., Brkić, K., and Bogunović, N. 2015. "A review of feature selection methods with applications." In 2015 38th International Convention on Information and Communication Technology, Electronics and Microelectronics, MIPRO 2015 – Proceedings, 1200–1205, Institute of Electrical and Electronics Engineers Inc.
- Julian, J.T., Young, J.A., Jones, J.W., Snyder, C.D., and Wright, C.W. 2009. "The use of local indicators of spatial association to improve LiDAR-derived predictions of potential amphibian breeding ponds." *Journal of Geographical Systems*, Vol. 11(No. 1): pp. 89–106. doi:10.1007/s10109-008-0074-4.
- Kavzoglu, T., and Colkesen, I. 2009. "A kernel functions analysis for support vector machines for land cover classification." *International Journal of Applied Earth Observation and Geoinformation*, Vol. 11(No. 5): pp. 352–359. doi:10.1016/j.jag.2009.06.002.
- Kuhn, M., and Johnson, K. 2013. *Applied predictive modeling*. New York: Springer.
- Kuhn, M. 2019. "The Caret Package." <http://topepo.github.io/caret/index.html>.
- Lang, M.W., and McCarty, G.W. 2009. "LiDAR intensity for improved detection of inundation below the forest canopy." *Wetlands*, Vol. 29(No. 4): pp. 1166–1178. doi:10.1672/08-197.1.
- Lathrop, R.G., Montesano, P., Tesauro, J., and Zarate, B. 2005. "Statewide mapping and assessment of vernal pools: A New Jersey case study." *Journal of Environmental*

- Management*, Vol. 76(No. 3): pp. 230–238. doi:10.1016/j.jenvman.2005.02.006.
- Leibowitz, S.G. 2003. “Isolated wetlands and their functions: An ecological perspective.” *Wetlands*, Vol. 23(No. 3): pp. 517–531. doi:10.1672/0277-5212(2003)023[0517:IWATFA.2.0.CO;2]
- Leonard, P.B., Baldwin, R.F., Homyack, J.A., and Wigley, T.B. 2012. “Remote detection of small wetlands in the Atlantic Coastal Plain of North America: Local relief models, ground validation, and high-throughput computing.” *Forest Ecology and Management*, Vol. 284(November): pp. 107–115. doi:10.1016/j.foreco.2012.07.034.
- Lindsay, J.B. 2005. “The terrain analysis system: A tool for hydro-geomorphic applications.” *Hydrological Processes*, Vol. 19(No. 5): pp. 1123–1130. doi:10.1002/hyp.5818.
- Lindsay, J. B. 2016. “Whitebox geospatial analytical tools.” <https://jblindsay.github.io/ghrg/Whitebox/download.shtml>.
- Ma, L., Cheng, L., Li, M., Liu, Y., and Ma, X. 2015. “Training set size, scale, and features in geographic object-based image analysis of very high resolution unmanned aerial vehicle imagery.” *ISPRS Journal of Photogrammetry and Remote Sensing*, Vol. 102(April): pp. 14–27. doi:10.1016/j.isprsjprs.2014.12.026.
- Ma, L., Fu, T., Blaschke, T., Li, M., Tiede, D., Zhou, Z., Ma, X., and Chen, D. 2017a. “Evaluation of feature selection methods for object-based land cover mapping of unmanned aerial vehicle imagery using random forest and support vector machine classifiers.” *ISPRS International Journal of Geo-Information*, Vol. 6(No. 2): pp. 51–62. doi:10.3390/ijgi6020051.
- Ma, L., Li, M., Ma, X., Cheng, L., Du, P., and Liu, Y. 2017b. “A review of supervised object-based land-cover image classification.” *ISPRS Journal of Photogrammetry and Remote Sensing*, Vol. 130(August): 277–293. doi:10.1016/j.isprsjprs.2017.06.001.
- Markle, C.E., and Chow-Fraser, P. 2014. “Habitat selection by the Blanding’s Turtle (*Emydoidea blandingii*) on a protected island in Georgian Bay, Lake Huron.” *Chelonian Conservation and Biology*, Vol. 13(No. 2): pp. 216–226. doi:10.2744/CCB-1075.1.
- Maxwell, A.E., Warner, T.A., and Fang, F. 2018. “Implementation of machine-learning classification in remote sensing: An applied review.” *International Journal of Remote Sensing*, Vol. 39(No. 9): pp. 2784–2817. doi:10.1080/01431161.2018.1433343.
- Millard, K., and Richardson, M. 2013. “Wetland mapping with LiDAR derivatives, SAR polarimetric decompositions, and LiDAR–SAR fusion using a random forest classifier.” *Canadian Journal of Remote Sensing*, Vol. 39(No. 4): pp. 290–307. doi:10.5589/m13-038.
- Ontario Ministry of Natural Resources and Forestry. 2014. “Ontario wetland evaluation system: Southern manual, 3rd edition.” <https://files.ontario.ca/environment-and-energy/parks-and-protected-areas/ontario-wetland-evaluation-system-southern-manual-2014.pdf>.
- Ontario Ministry of Natural Resources and Forestry. 2020. “Imagery user guide.” https://www.sdc.gov.on.ca/sites/MNRF-PublicDocs/EN/CMID/Ontario_Imagery_User_Guide.pdf.
- Rampi, L.P., Knight, J.F., and Pelletier, K.C. 2014. “Wetland mapping in the Upper Midwest United States: An object-based approach integrating LiDAR and imagery data.” *Photogrammetric Engineering & Remote Sensing*, Vol. 80(No. 5): pp. 439–449. doi:10.14358/PERS.80.5.439.
- Reutebuch, S.E., Mc Gaughey, R.J., Andersen, H.E., and Carson, W.W. 2003. “Accuracy of a high-resolution LiDAR terrain model under a conifer forest canopy.” *Canadian Journal of Remote Sensing*, Vol. 29(No. 5): pp. 527–535. doi:10.5589/m03-022.
- Riley, J.W., Calhoun, D.L., Barichivich, W.J., and Walls, S.C. 2017. “Identifying small depressional wetlands and using a topographic position index to infer hydroperiod regimes for pond-breeding amphibians.” *Wetlands*, Vol. 37(No. 2): pp. 325–338. doi:10.1007/s13157-016-0872-2.
- Semlitsch, R.D., and Bodie, J.R. 1998. “Are small, isolated wetlands expendable?” *Conservation Biology*, Vol. 12(No. 5): pp. 1129–1133. doi:10.1046/j.1523-1739.1998.98166.x.
- Tian, S., Zhang, X., Tian, J., and Sun, Q. 2016. “Random forest classification of wetland landcovers from multi-sensor data in the arid region of Xinjiang, China.” *Remote Sensing*, Vol. 8(No. 11): pp. 954–968. doi:10.3390/rs8110954.
- Wu, Q., Lane, C., and Liu, H. 2014. “An effective method for detecting potential woodland vernal pools using high-resolution LiDAR data and aerial imagery.” *Remote Sensing*, Vol. 6(No. 11): pp. 11444–11467. doi:10.3390/rs6111444.